Inorganica Chimica Acta 457 (2017) 7–18

Contents lists available at ScienceDirect

Inorganica Chimica Acta

journal homepage: www.elsevier.com/locate/ica

Research paper

Three structurally related Copper complexes with two isomers: DNA/BSA binding ability, DNA cleavage activity and excellent cytotoxicity

Dong-Yan Zhang [a,c,1], Yan Nie [b,1], Hui Sang [b], Jing-Jing Suo [a,c], Zong-Jin Li [b], Wen Gu [a,c], Jin-Lei Tian [a,c,*], Xin Liu [a,c], Shi-Ping Yan [a,c]

[a] Department of Chemistry, Nankai University, Tianjin 300071, PR China
[b] Medical School of Nankai University, Nankai University, Tianjin 300071, PR China
[c] Key Laboratory of Advanced Energy Materials Chemistry (MOE), Nankai University, Tianjin 300071, PR China

ARTICLE INFO

Article history:
Received 5 June 2016
Received in revised form 25 November 2016
Accepted 1 December 2016
Available online 2 December 2016

Keywords:
Copper complexes
DNA cleavage
Anti-cancer ability
ROS
Caspase-3

ABSTRACT

Three Cu(II) complexes of $[Cu(\mathbf{L^1})(Br)_2]\cdot CH_3CN$ (**1**), $[Cu(\mathbf{L^2})_2(OAc)](PF_6)\cdot 2C_2H_5OH$ (**2**), and $[Cu(\mathbf{L^1})(\mathbf{L^2})](PF_6)_2$ (**3**) ($\mathbf{L^1}$ = 2-(6-(pyridine-2-yl)-4-*p*-tolylpyridin-2-yl)pyridine, $\mathbf{L^2}$ = 2-(4-(pyridine-2-yl)-6-*p*-tolylpyridin-2-yl)pyridine) were designed and synthesized as anti-cancer drugs. All complexes were structurally characterized by X-ray crystallography showing that three complexes were the mononuclear compounds with the triclinic crystal system $p\bar{1}$ space group. The interaction between each of these three complexes and calf thymus DNA (CT-DNA) was investigated via spectroscopic techniques and viscosity measurement, which indicated that these complexes could bind to CT-DNA by intercalation. Moreover, DNA cleavage experiment showed that, in the natural light under an aerobic environment, all complexes could cleave DNA in the absence of exogenous oxidant agent, and that singlet oxygen ($^1O_2$) might serve as the major cleavage active species. Protein binding experiment indicated that **1**–**3** could bind to bovine serum albumin (BSA) with moderate bonding via the static quenching mechanism. In addition, the IC50 values of these three complexes were significantly lower which denoted highly anti-cancer activities in comparison to cisplatin. And each of these complexes could individually inhibit proliferation potential of cancer cells by promoting G1-phase cell cycle arrest (G1 arrest) and inducing apoptosis through the production of reactive oxygen species (ROS) and the activation of caspase-3

1. Introduction

According to statistics, the number of people diagnosed with cancer and people died from cancer has been considerably increased during the past several decades [1,2]. However, the emergence of different kinds of anti-cancer regimens and potential anti-cancer drugs, such as cisplatin, have many drawbacks like general toxicity, nonspecific targeting and acquired drug resistance [3–6]. Thus, researchers now face their biggest challenge of developing novel anti-cancer therapies. Metal-based complexes served as anti-cancer drugs have attracted a great deal of attention of researchers because the metal ions play important roles in biological processes [7]. DNA is the primary pharmacological target of many metal-based drugs, hence exploring the interaction between metal complexes and DNA is of the most importance in understanding the mechanism of the treatment for cancer. Moreover, studies showed that transition metal complexes with DNA cleavage activity could be promising DNA structural probes and therapeutic agents [8–10].

Transition metal complexes have been synthesized and developed rapidly for chemotherapeutic applications attributing to their various coordination modes, redox behaviors, feasible substitution kinetic pathways, and highly anti-cancer activity [11]. Many transition metal complexes (such as Ru, Ln, V, Co, Zn, Cu, etc.) have been reported for their DNA cleavage activity, DNA/BSA binding ability and cytotoxicity [12–17]. Among those transition metal compounds, copper complexes have shown broad prospects as the anti-cancer drugs for the following reasons: copper is an essential element related to life process and an active component in various bio-enzymes; Cu(II) ion is easy to form complex with ligands; Cu(II) ion itself own redox potential and can produce ROS when they participate in the physiological reaction [18–21].

In the field of Cu(II) compounds acting as anti-cancer agent, complexes combined with polypyridine ligands which have aro-

* Corresponding author at: Department of Chemistry, Nankai University, Tianjin 300071, PR China.
E-mail addresses: tiant@nankai.edu.cn (J.-L. Tian), liuxin64@nankai.edu.cn (X. Liu).
[1] Both authors contributed equally to this work.

http://dx.doi.org/10.1016/j.ica.2016.12.002
0020-1693/

maticity and strong coordination ability with Cu(II) ions played the most important roles [22,23]. One of the most widely studied polypyridine ligands are terpyridyl and its derivatives. According to the reported literatures, terpyridine ligands can inhibit protein kinase activity and have cytotoxicity against several human tumor cell lines because the terpyridine could partly form a conjugated aromatic ring system with a relatively planar structure [24,25]. In recent years, a series of Cu(II) complexes based on terpyridine and its derivatives have been reported as potent DNA cleavage agents, and these derivatives with different substituent groups on the 4 site of the middle pyridine ring of terpyridine have been designed and synthesized in order to enhance the selectivity towards tumor cell as well as improve the anti-cancer activity [26,27]. Guo and co-workers reported a mitochondrion-targeting copper complex ([Cu(ttpy-tpp)Br_2]Br, ttpy-tpp = 4′-p-tolyl-(2,2′:6′,2″-terpyridyl)triphenyl phosphonium bromide). As a triphenyl phosphate (TPP) group was added to the 4 site of the middle pyridine ring of terpyridine, the complex could specifically identify the mitochondrion when it accessed to the tumor cells [28].

All the above facts stimulated our interest in the present work on describing the synthesis of two isomers: **L^1** = 2-(6-(pyridine-2-yl)-4-p-tolylpyridin-2-yl)pyridine and **L^2** = 2-(4-(pyridine-2-yl)-6-p-tolylpyridin-2-yl)pyridine suitable to coordinate metal ions. The two molecules act as tridentate ligands to the Copper(II) ion through the three heterocycle N atoms. Three Cu(II) compounds were synthesized and characterized by spectroscopic techniques and X-ray diffraction, which showed that they were mononuclear compounds with five-coordinated ligands, and were similar to the reported complexes with tripyridine ligands [29,30]. And there is a significant difference between the ligands used in our study and previously investigation. The main objective of this work is to determine the cytotoxicity of these new complexes and study the possible mechanisms action as anti-cancer drugs. UV-visible spectroscopy, fluorescence spectral titration and viscosity measurement showed that the three complexes had a strong binding affinity to DNA than previously reported Copper(II) complexes. Spectrum experiments revealed that complexes could combine with BSA. Three Copper(II) compounds also showed good DNA cleavage activity in the absence of exogenous oxidants, and they could generate singlet oxygen ($^1O_2$) in the natural light under an aerobic environment, which was consisted with previous reports [31–36]. All these complexes exhibited excellent anti-cancer potency with considerably lower IC 50 values against three human tumor cell lines in comparison to cisplatin. Further tests with the aim to explore the mechanisms behind the enhanced anti-cancer activity were also performed.

2. Experimental

2.1. Materials and measurements

Cisplatin, $Cu(OAc)_2{\cdot}2H_2O$, NH_4PF_6 and all solvents were purchased from Aldrich Co. Solution of the Cu(II) complexes and other reagents used for strand scission were prepared freshly in triple-distilled water before use. Solvents used in this research were purified by standard procedures. Ultra-pure MilliQ water (18.24 MΩ cm) was used in all experiments. Ethidium bromide (EB), agarose, bovine serum albumin (BSA), calf thymus DNA (CT-DNA), pBR322 plasmid DNA and biological stains were purchased from Sigma. Tris–HCl buffer solution was prepared using deionized sonicated triple-distilled water. Human breast cancer cell line (MDA-MB-231), human epithelial cervical cancer cell line (HeLa), and human lung cancer cell line (A549) were obtained from the American Type Culture Collection (Rockville, MD, USA).

^{1}H NMR spectra were recorded on a Bruker 400 (1H/400 MHz) spectrometer. Infrared spectroscopy on KBr pellets was performed on *a Bruker Vector 22* FT-IR spectrophotometer in the 4000–400 cm^{-1} range. Electrospray ionization mass spectrometry (ESI-MS) was obtained on Agilent 6520 top of flight liquid chromatography/mass spectrometry. In our work, ESI-MS experiment was operated in DMF solution which was attenuated by C_2H_5OH. UV absorption was measured on a *JASCO V-570* spectrophotometer. Fluorescence spectral data were acquired on a *MPF-4* fluorescence spectrophotometer at room temperature. Viscosity measurements were experimented on an Ubbelodhe viscometer at a constant temperature (37.0 ± 0.1 °C) in a thermostatic water-bath. The Gel Imaging and documentation DigiDoc-It System of DNA cleavage were assessed using Labworks Imaging and Analysis Software (UVI, UK). MTT assay was performed on Glomax-multi detection system (Promega, USA). HE and Hoechst 33342 staining assay kit were purchased from KeyGEN Biotech (Nanjing, China). ROS detection experiment was performed using reactive oxygen species kit (Beyotime Biotech, Shanghai, China). Flow cytometry analysis was carried out with LSR Fortessa and CellQuest software (BD, USA).

2.2. Synthesis of L^1, L^2 and the Copper(II) complexes of **1–3**

2.2.1. Synthesis of L^1 and L^2

The syntheses of both **L^1** and **L^2** were based on literature procedure [24,37,38]. A mixture of acetamide (36.6 g, 0.6 mmol), ammonium acetate (23.6 g, 0.3 mmol), *p*-tolualdehyde (2.48 g, 20.6 mmol) and 2-acetylpyridine (5 g, 41.2 mmol) were heated at 160 °C with stirring for 2 h in 250 ml round-bottom flask, then the resulting solution was cooled to 120 °C, and the aqueous sodium hydroxide (10% solution, 20 ml) was added over 20 min with heating to 120 °C for 2 h. The black brown paste was formed when the solution was cooled to room temperature and filtered out, and then washed with water and cool C_2H_5OH. The obtained solid was dissolved into $CHCl_3$ and separated using column chromatography (Al_2O_3, *n*-hexane: ethyl acetate = 8:1, v/v), rotary evaporating and the white crystalline solid **L^1** and **L^2** were obtained, individually. The structure of **L^1** and **L^2** are shown in Scheme 1.

L^1 1.9 g, 20%, ^{1}H NMR (400 MHz, $CDCl_3$, 300 K): δ 8.78 (2H, s), 8.73 (2H, m), 8.69(2H, d), 7.88 (2H, td), 7.84 (2H, d), 7.39 (2H, dd), 7.36 (2H, d), 2.43 (3H, s) (Fig. S1A). Selected FT-IR (KBr, ν, cm^{-1}): 1584, 1466, 1392, 1113, 789, 619, 504. ESI-MS: m/z 324.15 for $[\mathbf{L^1} + H]^+$.

L^2: 1.1 g 12%, ^{1}H NMR (400 MHz, $CDCl_3$, 300 K): δ 8.83 (1H, s), 8.74 (1H, d), 8.72 (1H, s), 8.69 (1H, s), 8.66 (1H, s), 7.91 (1H, s), 7.86 (2H, d) 7.83 (1H, d), 7.36 (2H, q), 7.34 (1H, s), 7.31 (1H, s), 7.29 (1H, s), 2.43 (3H, s) (Fig. S1B). Selected FT-IR (KBr, ν, cm^{-1}): 1583, 1549, 1471, 1113, 779, 619, 501. ESI-MS: m/z 324.15 for $[\mathbf{L^2} + H]^+$.

2.2.2. Synthesis of $[Cu(L^1)(Br)_2]{\cdot}CH_3CN$ (**1**)

To a solution of **L^1** (64.6 mg, 0.2 mmol) in CH_3CN (10 ml) was added a solution of $CuBr_2$ (44.7 mg, 0.2 mmol) in CH_3OH (10 ml). The mixture solution was refluxed with stirring for 4 h, and then the reaction solution was cooled to room temperature and filter. Blue and bulk crystals suitable for X-ray diffraction were obtained by slow evaporation of the filtrate after several weeks. Yield: 55%. Selected FT-IR (KBr, ν, cm^{-1}): 1602, 1113, 619, 447. ESI-MS: m/z 466.99 for $[Cu(\mathbf{L^1})(Br)]^+$.

2.2.3. Synthesis of $[Cu(L^2)_2(OAc)](PF6){\cdot}2C_2H_5OH$ (**2**)

To a solution of **L^2** (129.2 mg, 0.4 mmol) in C_2H_5OH (10 ml) was added a solution of $Cu(CH_3COO)_2{\cdot}2H_2O$ (39.8 mg, 0.2 mmol) in C_2H_5OH (10 ml). The mixture solution was refluxed with stirring

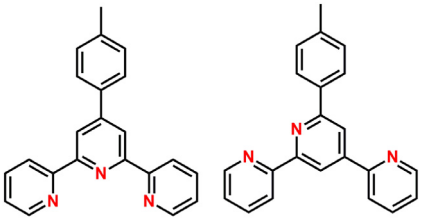

L^1 L^2

Scheme 1. Schematic molecular structures of **L1** and **L2**.

for 4 h, and then the reaction solution was cooled to room temperature and filter. Dark blue and clubbed crystals suitable for X-ray diffraction were obtained by slow evaporation of the filtrate after several weeks. Yield: 52%. Selected FT-IR (KBr, ν, cm^{-1}): 1613, 1472, 1113, 840, 619, 447. ESI-MS: m/z 709.21 for $[Cu(\mathbf{L^2})_2-H]^+$.

2.2.4. Synthesis of $[Cu(L^1)(L^2)](PF_6)_2$ (**3**)

To a solution of $\mathbf{L^1}$ (64.6 mg, 0.2 mmol) in CH_3OH (10 ml) was added a solution of $Cu(CH_3COO)_2{\cdot}2H_2O$ (39.8 mg, 0.2 mmol) in CH_3OH (5 ml). The mixture solution was refluxed with stirring for 2 h and a solution of $\mathbf{L^2}$ (64.6 mg, 0.2 mmol) in CH_3OH (10 ml) was added, then the reaction solution was refluxed with stirring for another 2 h and cooled to room temperature and filter. Dark blue and rhomboic crystals suitable for X-ray diffraction were obtained by slow evaporation of the filtrate after several weeks. Yield: 58%. Selected FT-IR (KBr, ν, cm^{-1}): 1608, 1109, 832, 619, 447. ESI-MS: m/z 709.21 for $[Cu(\mathbf{L^1})(\mathbf{L^2})-H]^+$.

2.3. X-ray crystallography

Diffraction data for **1**–**3** at 293 K, with a Bruker Smart 1000 CCD diffractometer using Mo-Kα radiation (λ = 0.71073Å) with the ω-2θ scan technique. An empirical absorption correction was applied to raw intensities [39]. The structures were analyzed by Olex2-1.2.3 and refined with full-matrix least-squares technique on F^2 using the Olex2-1.2.3 [40]. Hydrogen atoms were added according to the theory, and refined with intrinsic thermal factors. The crystallographic data and the parameters of structure refinement were summarized in Table 1. Selected bond angles and distances were listed in Table S1.

2.4. DNA-binding experiments

2.4.1. Absorption spectrophotometric and viscosity studies

The interaction of complexes **1**–**3** with CT-DNA was studied by UV spectroscopy, and the binding of DNA with complexes were operated at room temperature. The CT-DNA stock solutions were prepared in 5 mM Tris–HCl/50 mM NaCl buffer (pH = 7.2), showed a ratio of UV absorbance at 260 nm and 280 nm, (A_{260}/A_{280}, 1.8–1.9) indicating that the DNA was sufficiently free of protein [41]. The exact concentration of CT-DNA was determined according to its absorption intensity at 260 nm with a molar extinction coefficient of 6600 $M^{-1}cm^{-1}$ [42]. Then the solution was stored at 4 °C and used within 4 days. Specific methods were as follows: At room temperature, setting various parameters required (excitation wavelength 260 nm), 2 ml TE_1 solution was added to the sample pool and reference pool respectively, followed by scanning baseline and deducting background; then the appropriate amount of volume of complex solution was added to the sample pool (the maximum absorption peak the complexes should be around 1), the same volume of DMF solution was added to the reference pool, and the absorption peak of the complex was scanned; after that CT-DNA stock solution was added to the two pools with equal volume of scanning measurement of the absorption peak until the solution was saturated.

Viscosity experiments were carried out by using an Ubbelodhe viscometer maintained at a constant temperature at 37.0 ± 0.1 °C in a thermostatic water-bath. Flow time was measured with a digital stopwatch. Each sample was measured three times, and an average flow time was calculated. According to Cohen and Eisenberg [43,44], $\eta = (t - t_0)/t_0$ (where η is the viscosity of CT-DNA in the presence of complex, and η_0 is the viscosity of CT-DNA alone in 5 mM Tris buffer medium), the viscosity values were calculated from the observed flow time of CT-DNA containing solutions (t), duly corrected for that of the buffer alone (t_0), and then data were presented as $(\eta/\eta_0)^{1/3}$ versus [complex]/[DNA].

Table 1
Crystal data and structure refinement for complexes **1**–**3**.

Complex	1	2	3
Formula	$C_{24}H_{20}Br_2CuN_4$	$C_{50}H_{49}CuF_6N_6O_4P$	$C_{44}H_{34}CuF_{12}N_6P_2$
Mr	587.80	1006.46	1000.25
Crystal system	Triclinic	Triclinic	Triclinic
Space group	$p\bar{1}$	$p\bar{1}$	$p\bar{1}$
T/K	113 K	293(2) K	113.1500 K
a/Å	8.0291(16)	11.797(2)	10.472(2)
b/Å	12.058(3)	14.778(3)	14.319(3)
c/Å	12.756(3)	15.549(3)	14.895(3)
α/°	115.147(3)	108.49(3)	84.14(3)
β/°	91.128(4)	109.75(3)	69.76(3)
γ/°	96.029(3)	100.14(3)	77.01(3)
V/Å^3	1108.8(4)	2294.6(8)	2041.4(7)
Z	2	2	2
D/g/cm^3	1.761	1.457	1.627
μ/mm^{-1}	4.608	0.589	0.712
Reflections measured	5024	8094	9636
Independent reflections	14,307	16,289	21,297
R_{int}	0.0268	0.0383	0.0412
$R_1(I > 2\,\sigma\,(I))$	0.0275	0.0489	0.0491
$wR(F^2)(I > 2\,\sigma\,(I))$	0.0979	0.1149	0.1238
R_1(all data)	0.0320	0.0659	0.0708
$wR(F^2)$ (all data)	0.1005	0.1274	0.1426
Goodness of fit on F^2	0.824	0.999	0.840

2.4.2. Competitive binding experiments

Through fluorescence spectral method, the relative bindings of complexes to CT-DNA were studied with an EB-bound CT-DNA solution in 5 mM Tris–HCl/50 mM NaCl buffer (pH = 7.2). The fluorescence spectra intensity was at 602 nm (excite at 510 nm), which was carried out by titrating complexes into EB-DNA solution containing 2.4 μM EB and 48 μM CT-DNA.

2.4.3. DNA cleavage and mechanism studies

The implementation of DNA cleavage experiments was performed by agarose gel electrophoresis at 37.0 °C as follows: pBR322 DNA (0.1 μg/μL) was treated with complexes **1**–**3** in 50 mM Tris-HCl/18 mM NaCl buffer (pH = 7.2), and incubated for 3 h at 37.0 °C. Then the samples were electrophoresed for 2 h at 0.9% agarose gel into Tris-boric acid-EDTA buffer. After electrophoresis, the different DNA forms were visualized under UV light and photo-graphed. The cleavage efficiency was measured by determining the ability of the complex to convert the supercoiled (SC) DNA (Form I) to nicked circular (NC) DNA (Form II) and linear (LC) DNA (Form III) [45].

To investigate the cleavage mechanistic of pBR322DNA, different reagents such as hydroxyl radical scavengers (DMSO, KI), singlet oxygen quenchers (NaN_3, L-histidine), superoxide scavenger (SOD), hydrogen peroxide scavenger (catalase), chelating agent

(EDTA), minor groove scavenger (Methyl Green), and major groove scavenger (SYBR Green) were added into pBR322DNA solution prior to the addition of the complexes.

2.5. Protein binding studies

The investigation of interaction between BSA and complexes **1**–**3** were carried out by fluorescence quenching experiments. BSA solution (1.5 mM) were prepared in 10 mM phosphate buffer (pH = 7.0). The spectra of fluorescence quenching experiments were recorded at room temperature with the excitation wavelength of BSA at 280 nm (the emission wavelength at 342 nm) by keeping the concentration of BSA on a constant (29.4 μM) while varying the concentration of complex.

2.6. Cytotoxicity assessment by MTT assay

The influence of **1**–**3** and Cisplatin on the proliferation of cancer cells was measured using the MTT assay kit (Roche Diagnostics GmbH). Cells were seeded in 96-well plates at a density of 3000 cells/well and incubated for 24 h to allow the attachment. Then, these cells were incubated with Cu(II) complexes or DMF vehicle control with a gradient concentration in FBS-free medium for 24 h, then 50 μl of the MTT reagent was added to each well. After incubation for 3 h at 37 °C, the absorbance was measured at 560 nm using an enzyme linked immunosorbent assay reader (Promega, USA).

2.7. Morphological changes and nuclear fragmentation

Copper complexes induced morphological changes and nuclear chromatin condensation in MDA-MB-231 cells were evaluated by Hematoxyline-Eosin (HE) staining and Hoechst 33342 staining (KeyGEN Biotech, Nanjing, China). MDA-MB-231 cells were treated with **1**–**3** for 24 h at the concentration of IC_{50}. Then, cells were fixed with 4% paraformaldehyde for 20 min, washed in PBS, and stained with HE or Hoechst 33342 according to the manufacturer's protocol separately. After washing twice with PBS, HE staining manifested the morphological changes which were observed under a microscope, Hoechst 33342 staining showed the nuclear fragmentation which was observed under a fluorescent microscope (Olympus).

2.8. Measurement of ROS

To measure ROS generation, reactive oxygen species assay kit (Beyotime, Cat S0033, China) was used. MDA-MB-231 cells were seeded to 6-well plate at density of 2×10^5 cells/well. The following day (at ~ 80% confluence), cells were exposed to **1**–**3** at concentration of 1 μM for 24 h. Then cells were washed twice with sterile PBS. To each test sample, the ROS probe, DCFH-DA, was added according to the manufacture's instruction. After incubation for 20 min at 37 °C, cells were washed twice with sterile PBS. Following, those samples were observed under a fluorescent microscope (Olympus) at 100× magnification.

2.9. Flow cytometry analysis for apoptosis quantification

MDA-MB-231 cells seeded to 35 mm dishes at density of 2×10^5 cells/dish. The following day (at ~ 80% confluence), cells were treated with **1**–**3** at concentration of IC_{50} and were harvested at 24 h. Annexin V-FITC/propidium iodide (PI) double staining apoptosis detection kit (Bioscience, Mountain View, CA, USA) was used following the manufacture's protocol. Then, cells were analyzed immediately by flow cytometry (BD Biosciences, San Diego, CA, USA). The data were analyzed by using FlowJo 7.6 software.

2.10. Colony-forming assay

For colony-forming assays, single cell suspension of MDA-MB-231 cells were seeded into 6-well tissue culture plates at a density of 3000 cells/well and allowed to adhere overnight. Afterward, FBS-free culture medium containing Cu(II) compounds at their IC_{50} values was added to each well. After expose to these complexes for 24 h, cells were washed twice with sterile PBS and incubated at 37 °C in drug-free medium containing 10% FBS for 10 days. On the 10th day, cells were fixed with 4% paraformaldehyde and stained with 2% crystal violet in methanol.

2.11. Cell cycle assays

Cell cycle distributions at different stages were determined using cell cycle kit (BestBio). MDA-MB-231 cells were seeded to 6-well plate at density of 2×10^5 cells/well allowed to adhere overnight. Then cells were treated with **1**–**3** separately at IC_{50} value for 24 h. Then cells were harvested including the floating cells in the medium and fixed in 70% ethanol at 4 °C for 3 h. Ethanol was removed from the fixed cell through centrifugation at 1000 rpm for 5 min. Cell pellets were re-suspended in 1 ml **1**–**3** Banding Buffer containing 100 μg/ml RNAase and incubated with 1 ml PI staining solution (50 μg/ml) for 30 min at 4 °C in the dark according to the manufacture's instruction. Cell cycle distribution was investigated using BD AccuriR C6 Flow Cytometer. Data, in the form of a DNA histogram, were analyzed by using FlowJo 7.6 software.

2.12. Caspase-3 activation assay

The Caspase-3 activation was measured using Caspase-3 colorimetric assay kit (KeyGEN, China) following the manufacturer's protocol. Briefly, the MDA-MB-231 cells were incubated with compound **1**, **2** and **3** (1.5 μM) for 24 h, respectively. Then cells were harvested and lysates using lysis buffer containing DTT. Each sample of these cell lysates (200 μg per sample) were mixed with 2 × reaction buffer and probe for Caspase-3 at 37 °C for 4 h. D_{400} values were measured using an enzyme-linked immunosorbent assay reader (Promega, USA).

3. Result and discussion

3.1. Synthesis and characterization

Ligands $\mathbf{L^1}$ and $\mathbf{L^2}$ were prepared with the same method, and they were the isomeride (Scheme 1) and separated using column chromatography (Al_2O_3, *n*-hexane: ethyl acetate = 8:1, v/v). ^1H NMR spectra showed that they had no obvious difference (Fig. S1), and the value of ESI-MS was same: to $\mathbf{L^1}$, *m*/*z* 324.15 for $[\mathbf{L^1} + H]^+$, to $\mathbf{L^2}$, *m*/*z* 324.15 for $[\mathbf{L^2} + H]^+$. All the Cu(II) complexes were synthesized by reflux and slow evaporation at room temperature, and they all were mononuclear compounds with the triclinic crystal system $p\bar{1}$ space group. The results of ESI-MS analysis indicated these copper complexes kept stable in DMF solution, to **1**, 466.99 for $[Cu(\mathbf{L^1})(Br)]^+$; to **2**, 709.21 for $[Cu(\mathbf{L^2})_2\text{-}H]^+$ and to **3**, 709.21 for $[Cu(\mathbf{L^1})(\mathbf{L^2})\text{-}H]^+$.

3.2. X-ray crystal structure of complexes *1*–*3*

Complexes **1**–**3** have been structurally characterized by X-ray crystallography (Fig. 1), details of data collection conditions and parameters of refinement process were given in Table 1, the selected bond lengths and angles were given in Table S1, respectively, and the distances of π-π interaction (Fig. 2) about **1** and **2** were given in Table 2.

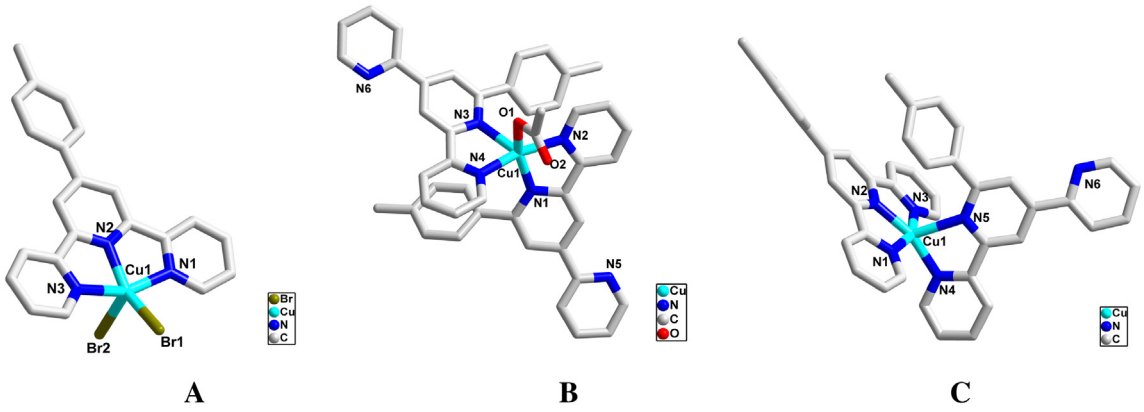

Fig. 1. The ORTEP diagram of coordination sphere for **1**–**3**, the solvent molecules and all hydrogen atoms are omitted for clarity. A is for **1**, B is for **2**, C is for **3**.

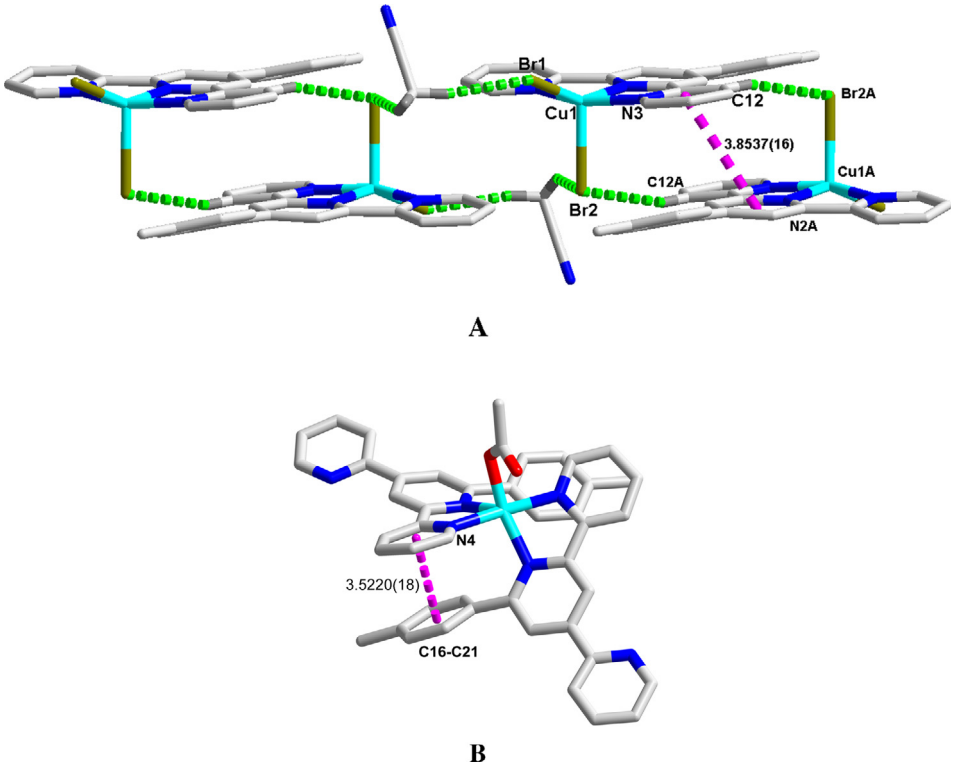

Fig. 2. A is the 1D lain structure of **1** with π-π interactions (purple) and hydrogen bond (green), B is the structure of **2** with π-π interactions (purple). (For interpretation of the references to color in this figure legend, the reader is referred to the web version of this article.)

Table 2
Intermolecular π-π interaction distances (Å).

π-π interactions	Plane A	Plane B	Distances
1			
Cg(A)—Cg(B)	N2—C6—C7—C8—C9—C10	N3—C11—C12—C13—C14—C15	3.8537(16)
2			
Cg(A)—Cg(B)	N4—C23—C24—C25—C26—C27	C16—C17—C18—C19—C20—C21	3.5220(18)

3.2.1. Crystal structure of $[Cu(L^1)(Br)_2]\cdot CH_3CN$ (**1**)

Complex **1** was the mononuclear compounds with the triclinic crystal system $p\bar{1}$ space group. The asymmetric unit of **1** was composed of one crystallographically independent Cu(II) ion, one $\mathbf{L^1}$ ligand, two bromide ions and one acetonitrile molecules. **1** was a mononuclear structure, as shown in Fig. 1A, Cu1 located in a five-coordinated environment completed by three nitrogen atoms (N1, N2 and N3) from $\mathbf{L^1}$ ligand and two bromide atoms (Br1 and Br2). The distance between metal and coordination atoms were: Cu(1)-N(1) = 2.049(2)Å, Cu(1)-N(2) = 1.963(2)Å, Cu(1)-N(3) = 2.054(2)Å, Cu(1)-Br(1) = 2.3914(6)Å and Cu(1)-Br(2) = 2.6163(6)Å. The selected angles between metal and coordination atoms were: Br(1)-Cu(1)-Br(2) = 107.069(16)°, N(2)-Cu(1)-Br(2) = 101.19(6)°, N(2)-Cu(1)-Br(1) = 151.73(6)° and N(1)-Cu(1)-N(3) = 156.88(8)°. The space configuration of five-coordinated complexes could be well defined by the τ value ($\tau = (\beta - \alpha)/60$ and α and β being the two largest coordination angles), τ = 0 for an ideal square pyramid as well as τ = 1 for an ideal triangular bipyramid [46,47]. For $[Cu(\mathbf{L^1})(Br)_2]$, the value of τ were equal to 0.09. So in the case of **1**, the Cu(II) square-pyramid were defined by the three nitro-gen-

donors of the $\mathbf{L^1}$ ligand and two bromide ligands. As shown in Fig. 2A, **1** could form two-double 1D chain structure with wake C-H···Br, and the distance of C12-H···Br2A and C (CH3CN)-H···Br1 were 2.817Å and 2.864Å, respectively [48]. Moreover, the π-π interactions were existed between the two-double, as shown in Fig. 2A. The center distance between the ring obtain N3 and the ring obtain N2A was 3.8537(16) Å (Table 2) and their dihedral angel was 7.143(102)°, suggesting the two rings obtain N3 and N2A exist π-π interactions [49].

3.2.2. Crystal structure of $[Cu(L^2)_2(OAc)](PF6)\cdot 2C_2H_5OH$ (**2**)

Single crystal X-ray analysis revealed that complex **2** crystallized in the monoclinic space group $p\bar{1}$ with one Cu(II) ion, two $\mathbf{L^2}$ ligands, one CH_3COO^- ion, one PF_6^- counter ion and two ethanol molecules in the asymmetric unit. As shown in Fig. 1B, **2** was a mononuclear structure and Cu1 located in a five-coordinated environment completed by four nitrogen atoms (N1, N2, N3 and N4) from two $\mathbf{L^2}$ ligands and one oxygen atom (O1) from CH_3COO^- ion. The distance between metal and coordination atoms were: Cu(1)-N(1) = 2.078(2)Å, Cu(1)-N(2) = 1.981(2)Å, Cu(1)-N(3) = 2.274(2)Å, Cu(1)-N(4) = 1.997(2)Å and Cu(1)-O(1) = 1.972(2)Å. The selected angles between metal and coordination atoms were: N(2)-Cu(1)-N(4) = 163.97(10)°, N(2)-Cu(1)-N(3) = 117.20(10)°, N(1)-Cu(1)-N(3) = 111.93(9)° and O(1)-Cu(1)-N(1) = 160.48(9)°. For the five-coordinated environment of $[Cu(\mathbf{L^2})_2(OAc)]$, the value of τ was equal to 0.06. So in the case of **2**, the square-pyramid of Cu (II) complex was defined by the two nitro-gendonors of the two $\mathbf{L^2}$ ligands and one oxygen atom by the acetic acid ligand. In addition, as shown in Fig. 2B, the center distance between the rings obtain N4 and C16-C21 was 3.5220(18) Å (Table 2) and their dihedral angel is 10.979(105)°, thus, the two rings exist π-π interactions [50].

3.2.3. Crystal structure of $[Cu(L^1)(L^2)](PF_6)_2$ (**3**)

The structure of **3** was sample and easy, single crystal X-ray analysis revealed that complex **3** crystallized in mononuclear structure with monoclinic space group $p\bar{1}$ with one Cu(II) ion, one $\mathbf{L^1}$ ligand, one $\mathbf{L^2}$ ligand, and two PF_6^- counter ions in the asymmetric unit. As shown in Fig. 1C, Cu1 located in a five-coordinated environment completed by five nitrogen atoms: N1, N2 and N3 from $\mathbf{L^1}$ ligand, and N4, N5 from $\mathbf{L^2}$ ligand. The distance between metal and five nitrogen atoms were: Cu(1)-N(1) = 2.047(2)Å, Cu(1)-N(2) = 1.930(2)Å, Cu(1)-N(3) = 2.031(2)Å, Cu(1)-N(4) = 2.001(2)Å and Cu(1)-N(5) = 2.277(2)Å. The selected angles between Cu (II) and N atoms were: N(2)-Cu(1)-N(5) = 118.72(9)°, N(3)-Cu(1)-N(1) = 158.53(9)° and N(2)-Cu(1)-N(4) = 162.77(9)°. For the five-coordinated environment of $[Cu(\mathbf{L^1})(\mathbf{L^2})]$, the value of τ was equal to 0.07. So in the case of **3**, the square-pyramid of Cu(II) complex was defined by the three nitro-gendonors of the $\mathbf{L^1}$ ligand and two nitro-gendonors of the $\mathbf{L^2}$ ligand.

3.3. DNA-binding experiments

3.3.1. Absorption spectrophotometric and viscosity studies

DNA-binding experiment of metal complexes to DNA is considered to be an essential step in the field of DNA cleavage study. UV-visible spectroscopy is known as a basic and reliable method to evaluate the binding ability of metal complexes with DNA. The absorption spectra of three complexes were characterized by intense π-π* ligand transitions in the UV and metal-to-ligand charge transfer (MLCT) transition in the visible region. After complex interacts with the base pairs of DNA [51], the π-π* transition energy would decrease and the transition probabilities are decreased as well as resulting in hypochromism. The CT-DNA binding ability of complexes **1**–**3** were conformed on the UV absorption

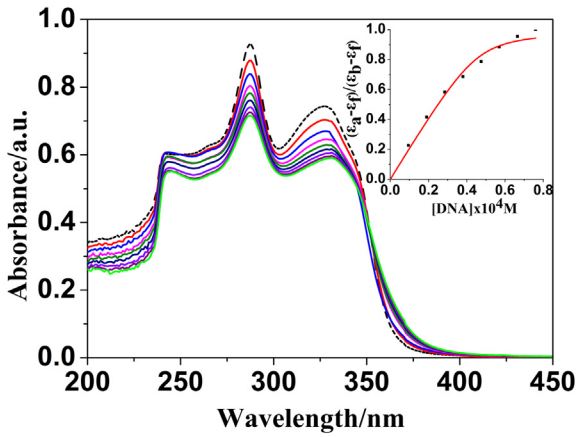

Fig. 3. Absorption spectra of complex **1** (37.5 μM) in the absence (black line) and presence (colored line) of increasing amounts of CT-DNA (9.5, 19, 28.5, 38, 47.5, 57, 66.5, 76 μM) in 5 mM Tris–HCl/50 mM NaCl buffer (pH = 7.2). The insert shows the least-squares fit of $(\varepsilon_a - \varepsilon_f)/(\varepsilon_b - \varepsilon_f)$ vs [DNA] for complex **1**.

while increasing concentration of CT-DNA stock solution into complex solution. As shown in Fig. 3 (Fig. S2), when increasing the concentration of CT-DNA to the solution of complex, the absorption dramatically decreased and the hypochromism of **1**–**3** was between 53% and 56%. In order to further confirm the binding strength of complex with CT-DNA, the intrinsic binding constants K_b were calculated from a nonlinear fitting according to the blow equation [52,53].

$$(\varepsilon_a - \varepsilon_b)/(\varepsilon_b - \varepsilon_f) = \{b - (b^2 - 2K_b^2 C_t[\mathrm{DNA}]/s)^{1/2}\}/2K_bC_t \quad (1a)$$

$$b = 1 + K_bC_t + K_b[\mathrm{DNA}]/2s \quad (1b)$$

Where C_t is the concentration of complex; [DNA] is the concentration of DNA; s is the binding site size of DNA which combine with complex; ε_a, ε_b and ε_f are the molar absorption coefficient and ε_a is the extinction coefficient observed for the charge-transfer absorption band at a given DNA concentration; ε_b is the extinction coefficient of the complex when fully bound to DNA; ε_f is the extinction coefficient of the complex free in solution. The data of K_b and s were presented as $(\varepsilon_a - \varepsilon_f)/(\varepsilon_b - \varepsilon_f)$ vs [DNA] in Fig. 3 (Fig. S2) and Table 3. As shown in Table 3, the binding constant of complexes to DNA as follows: $K_b = 6.36 \times 10^5$ for **1**, $K_b = 3.82 \times 10^5$ for **2** and $K_b = 1.26 \times 10^4$ for **3**. When compared the K_b values of the three Cu complexes to the reported Copper(II) complexes [54,55] with the same structure ($K_b = 2.02 \sim 6.04 \times 10^4$, $K_b = 2.3 \sim 3.3 \times 10^5$), results showed that although all the Cu(II) compounds were the mononuclear compounds with five-coordinated, owing to the major ligand had the difference in the structures and the small molecule ions were different. And the interaction between the complexes and DNA suggested this difference. Moreover, the magnitude of the K_b values of **1**–**3** were between 10^4 and 10^5, the value of DNA binding constant about **1**–**3** was less than the classical binding constant (10^7 M^{-1}) of EB, which suggested that the interaction of three complexes with DNA was a moderate strength intercalative mode. And **1** exhibited a slightly stronger DNA binding affinity in compar-

Table 3
Fluorescence spectral properties of complex **1**–**3** bound to CT–DNA.

Complex	$K_b(M^{-1})$	s	$\Delta\varepsilon$ (%)	K_{app} (M^{-1})
1	6.36×10^5	0.06	54.7	1.25×10^{12}
2	3.82×10^5	0.05	53.7	5.98×10^{11}
3	1.26×10^4	0.11	55.7	2.04×10^{12}

K_b: intrinsic equilibrium DNA binding constant; s: binding site size value; $\Delta\varepsilon$: the trend in hypochromism; K_{app}: apparent DNA binding constant; estimated errors for the constants are ± 5%.

ison with **2** and **3**. The reason might be that **1** owned one ligand of better planarity than other compounds. Thus, the space hindrance of **1** was small than other compounds when interacted with DNA.

Compared with the UV-visible spectroscopy, viscosity measurement is an effective method to study the small molecule interaction between complexes and DNA in the form of a more accurate and more effective method of fluid mechanics [56]. When complexes bound to DNA via insertion, the distance between DNA base pairs will increase, which leads the increased length of DNA chain together with increased viscosity [57]. The ratio of three complexes relative specific viscosity $(\eta/\eta_0)^{1/3}$ versus [complex]/[DNA] for **1**, **2** and **3** were given in Fig. 4. When added the complex concertration into DNA solution, the relative viscosity of DNA increased efficiently, suggesting that compounds could bind to DNA by intercalation.

3.3.2. Competitive binding experiments

Fluorescence spectral titration measurement was used to further investigate the mode of binding of the complexes with DNA, via intercalation or groove binding. Fluorescence quenching assay using EB-bound DNA as probe is an effective method to study the mode of binding of the complexes to DNA. EB, a planar cationic dye, is a typical indicator of intercalation, which could form soluble complexes with CT-DNA and then emit intense fluorescence [58]. When add a second DNA intercalate agent that could replace EB from DNA-bound EB system into EB-DNA solution, the fluorescence of system will be quenched as the fact that free EB molecules are readily quenched by surrounding water molecules [59]. The fluorescence quenching spectra of **1**–**3** with EB-bound DNA were shown in Fig. 5 (Fig. S3). Emission band at 610 nm displayed more obvious hypochromism when the increasing concentrations of **1**–**3**. The quenching tendency illustrated that the quenching of EB system by complex was in agreement with the classical linear Stern–Volmer equation [60].

$$I_0/I = 1 + K_{sv}[Q] \quad (2a)$$

$$K_{EB}[\mathrm{EB}] = K_{app}[\mathrm{complex}] \quad (2b)$$

Where I_0 and I represent the fluorescence intensities in the absence and presence of quencher, $[Q]$ is the concentration of quencher, K_{sv} is the Stern-Volmer dynamic quenching constant. Here K_{EB} is the binding constant of EB to DNA [$K_{EB} = 1.0 \times 10^7\ M^{-1}$, ([EB] = 2.4 μM)], [complex] is the concentration value of complex at a 50% reduction of fluorescence intensity of EB and K_{app} is the apparent DNA binding constant. The data of K_{sv} was presented as I_0/I vs [Q] in the Fig. 5 (Fig. S3) and Table 3. As shown in Table 3, the magnitude of the K_{app} values of **1**–**3** ware between 10^{11} and 10^{12}. As expected, the competitive binding of three complexes to DNA with EB could result in displacement of EB as well as dramatic decrease of emission intensity.

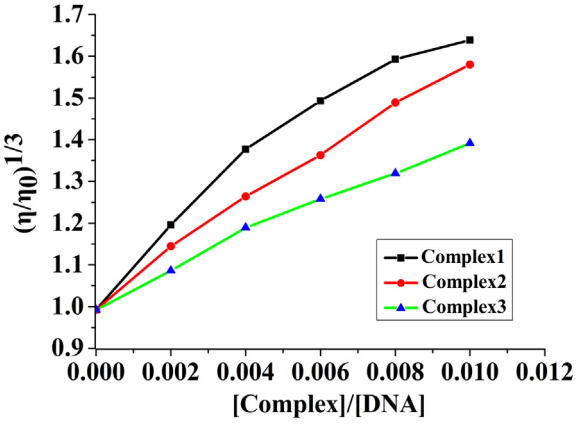

Fig. 4. Effects of increasing amount of complex on relative viscosity of CT-DNA at 37.0 ± 0.1 °C conditions: [DNA] = 1 mM, [complex] = 0–0.01 mM.

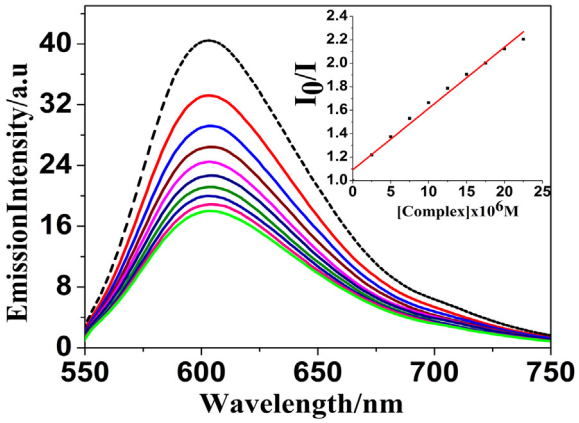

Fig. 5. Emission spectra of EB bound to CT-DNA in the absence (dashed line) and presence (solid lines) of complex **1** (0–22.5 μM) in 50 mM Tris–HCl/18 mM NaCl buffer (pH = 7.2).Inset: the plot of I_0/I versus [complex].

3.3.3. DNA cleavage and mechanism studies

In order to detect the DNA cleavage activities of the complexes, agarose gel electrophoresis for the cleavage of pBR322 plasmid DNA was performed in the buffer (50 mM Tris-HCl/18 mM NaCl, pH = 7.2) under the natural light in an aerobic environment without the exogenous oxidant agent. All these complexes could relax the supercoiled circular (SC) form of plasmid DNA into nicked circular (NC) form and/or linear form. Fig. 6 showed the cleavage activity of **1**–**3** to pBR322 DNA at different concentrations, and different cleavage patterns (Form I, Form II and Form III) were observed after the samples were subjected to electrophoresis. Form I is the supercoiled structure without cleaving by complex which migrates at the fastest rate, Form II has only one incision on the one strand cleaved by complex which moves at the slowest rate, and Form III is a linear structure with the rate of migration

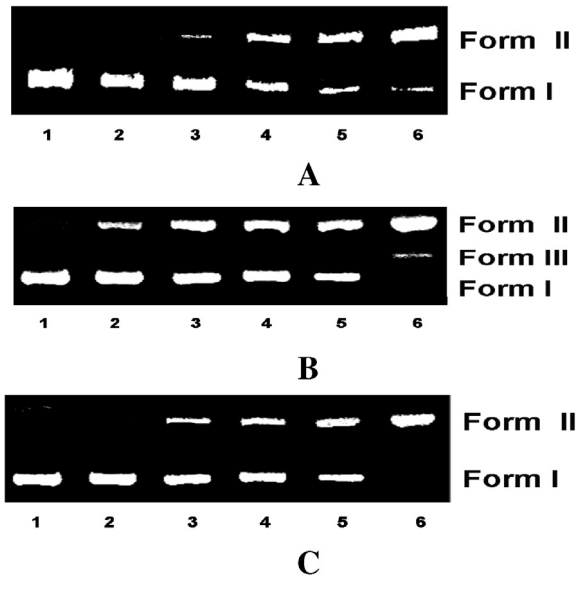

Fig. 6. Cleavage of plasmid pBR322 DNA (0.1 μg/μL) at different concentrations of complex **1** (A), **2** (B) and **3** (C) after 3 h incubation at 37 °C; Line 1: DNA control; Line 2–6: DNA + complex (5, 20, 35, 50, 65, 80 μM).

Fig. 7. Agarose (1%) gel electrophoresis showing cleavage of pBR322 DNA (200 ng) by complex **2** (65 μM) in different conditions for anincubation time of 3.0 h at 37 °C. Lane 1, DNA control; Lane 2, DNA + **2**; Lane 3, DNA + **2** + KI (1 mM); Lane 4, DNA + **2** + DMSO (1 mM); Lane 5, DNA + **2** + NaN_3 (20 mM); Lane 6, DNA + **2** + L-histidine (20 mM); Lane 7, DNA + **2** + SOD (20U/mL); Lane 8, DNA + **2** + Catalase (20U/mL); Lane 9, DNA + **2** + EDTA (10 mM); Lane 10, DNA + **2** + Methyl Green; Lane 11, DNA + **2** + SYBR Green.

Table 4
The quenching constant, binding constant and number of binding sites for the interactions of complex **1**–**3** with BSA.

Complex	K_{sv} (M^{-1})	K_q (M^{-1} s^{-1})	K_{bin} (M^{-1})	n
1	6.1×10^4	6.1×10^{12}	5.25×10^4	0.99
2	4.5×10^4	4.5×10^{12}	2.4×10^7	1.61
3	3.9×10^4	3.9×10^{12}	3.8×10^3	0.79

K_{sv}: quenching constant; K_q: quenching rate constant; K_{bin}: binding constant of compound with DNA; n: the number of binding sites; estimated errors for the constants are ± 5%.

between the rate of Form I and Form II. As shown in Fig. 6, obvious DNA cleavage could be detected at the concentration of 35 μM for **1**, 5 μM for **2** and 20 μM for **3**. Moreover, when the concentration was increased to 65 μM for **2**, the Form III appeared, suggesting **2** had the best cleavage activity.

In order to authenticate the cleavage mechanism of pBR322 DNA by complexes **1**–**3**, several ROS inhibiting agents, including hydrogen radical scavenger (KI, DMSO), singlet oxygen quenchers (NaN_3, L-histidine), superoxide scavenger (SOD, superoxide dismutase), peroxide anion scavenger (catalase) and chelating agent (EDTA), big groove scavenger (Methyl Green), and small groove scavenger (SYBR Green) were added into pBR322DNA solution prior to the addition of the complexes [61]. As showed in Fig. 7 (Fig. S4), singlet oxygen quenchers (L-histidine) (lane 6 of all) markedly inhibited the cleavage activity of all complexes, suggesting that singlet oxygen ($^1O_2$) was the major cleavage active species in the cleavage reaction. In addition, the chelating agent (EDTA) (lane 9 of all) had the ability to inhibit DNA cleavage efficiently, which indicated Cu^{2+} played a key role in the DNA destruction.

3.4. Protein binding studies

In blood plasma, Serum albumin (SA) is the main protein acting as an important role in drug transport and drug metabolism and constitutes ~ 55% of the total protein. The study of the interaction between metal complexes and proteins is the basis for the investigation of how the metal drugs affect the cancer cells. In our study, bovine serum albumin (BSA) was used because its structure is similar to human serum albumin (HSA) and it can be easily obtained [62,63]. BSA has three fluorophores: tryptophan, tyrosine and phenylalanine, and the intrinsic fluorescence of BSA is mainly attributed to tryptophan [64]. Fluorescence quenching measurements have been widely used to study the interaction of metal complexes or small molecules with proteins [65]. Brustein etc [66] believed that the greatest fluorescence emission peak position of tryptophan was sensitive to the environment. Fig.S5 showed the effect of **1**–**3** on fluorescent intensity of BSA at room temperature, a solution of BSA (29.4 μM) was titrated with varying concentrations of complexes, and fluorescence intensity was recorded in the range of 290–500 nm upon excitation at 280 nm. A gradual decrease in fluorescence intensity as well as a blue shift in wavelength were observed after increasing concentration of compounds. To further study quenching process, fluorescence quenching data were analyzed with Stern-Volmer equation (3a) and Scatchard equation (3b) [67].

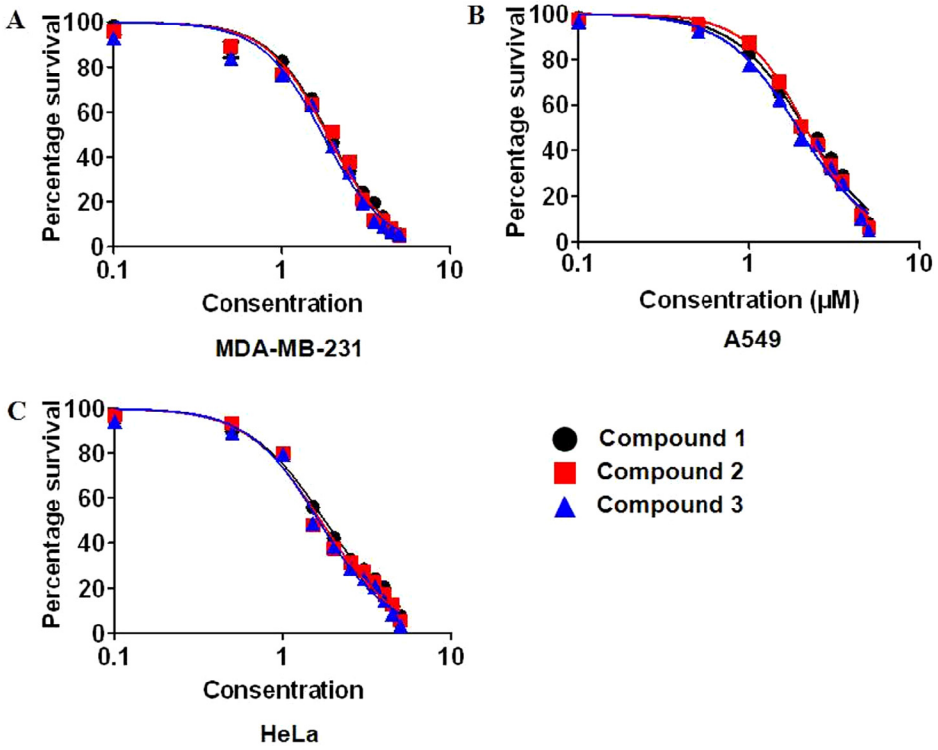

Fig. 8. MTT assay of **1**–**3** with MDA-MB-231 (A), A549 (B) and HeLa (C) cells.

$$I_0/I = 1 + K_{sv}[Q] = K_q\tau_0[Q] \quad (3a)$$

$$\lg[(I_0 - I)/I] = \lg K_{bin} + n\lg[Q] \quad (3b)$$

Where I_0 and I are the fluorescence intensities of the fluorophore in the absence and presence of quencher, respectively, K_q is the quenching rate constant, τ_0 the average life-time of the biomolecule without quencher (about 10^{-8} s), K_{bin} is binding constant of compound with DNA and n is the number of binding sites. As showed in Fig. S6, K_{sv} was observed by using the plot of I_0/I versus [Q], and the number of binding sites (n) and binding constant (K_{bin}) were obtained from the plot of lg(I_0-I)/I versus lg[Q]. In Table 4, the magnitude of the K_{bin} values of **1**–**3** were between 10^3 and 10^7, and the magnitude of the K_q was 10^{12}, suggesting the complexes had moderate binding activities to BSA at room temperature.

3.5. Cytotoxicity Assessment by MTT assay

The cytotoxicity of **1**–**3** on the growth of cancer cells were measured using the MTT assay. Cells in the control group and treatment groups were seeded in 96-well plates at a density of 3000 cells/well and incubated for 24 h to allow the attachment. Cytotoxic effects of these complexes on different cancer cell lines (MDA-MB-231, A549, and HeLa) were determined and showed in Fig. 8. The results from MTT assay indicated that these metal chelating compounds significantly reduced the viability of cancer cells within 24 h in a dose-dependent manner. The IC_{50} values of these three complexes on different cells at 24 h were showed in Table 5. The cytotoxicity of **1**–**3** on MDA-MB-231, A549 and HeLa cells were similar and the range of IC_{50} values were about 1.7–2.1 μM. In addition, the cytotoxic effects of cisplatin on these cancer cells in comparison to **1**–**3** were detected and showed in Table 5. The result suggested that the cytotoxic effects of **1**–**3** were more efficient than cisplatin. Further, the anti-cancer effects of these complexes were proved by the colony-forming assay, as shown in Fig. 9D, compared with the control cell, the number of live cell was decreased obviously when cells were treated with **1**–**3** for 24 h. Thus, these three cooper complexes may have the potential to develop into anti-cancer agents.

Table 5
IC_{50} values of **1**–**3** and Cisplation in MDA-MB-231 (**A**), A549 (**B**) and HeLa (**C**) cancer cells.

Complex	MDA-MB-231	A549	HeLa
	IC_{50} (μM)	IC_{50} (μM)	IC_{50} (μM)
1	1.9 ± 0.1	2.1 ± 0.2	2.0 ± 0.3
2	1.8 ± 0.2	2.1 ± 0.2	1.8 ± 0.1
3	1.7 ± 0.1	1.9 ± 0.1	1.9 ± 0.1
Cisplation	5.2 ± 0.6	8.9 ± 0.5	3.4 ± 0.8

3.6. Cell apoptosis analysis and attestation

Based on HE staining, morphological changes, such as the condensed and marginalized chromatin, could be observed after cells were exposing to the cooper complexes for 24 h, suggesting the initial apoptosis in MDA-MB-231 cells [68,69]. Hoechst 33342 staining further confirmed the nuclear chromatin condensation in MDA-MB-231 cells using fluorescence microscopy. As shown in Fig. 9 (A and B), compared with the control cells, cells treated with **1**–**3** for 24 h showed stronger blue fluorescence under a fluorescent microscope at 100X magnification, which suggested three cooper complexes had the ability of inducing the cell apoptosis.

Several reports indicated that the cell apoptosis pathway induced by complex might be dependent on ROS generation [70,71]. Besides, according to the previous study in our work, copper compounds could generate singlet oxygen ($^1O_2$) in the DNA cleavage reaction. Therefore, the experiment on measurement of ROS in the cell apoptosis pathway induced by complexes was

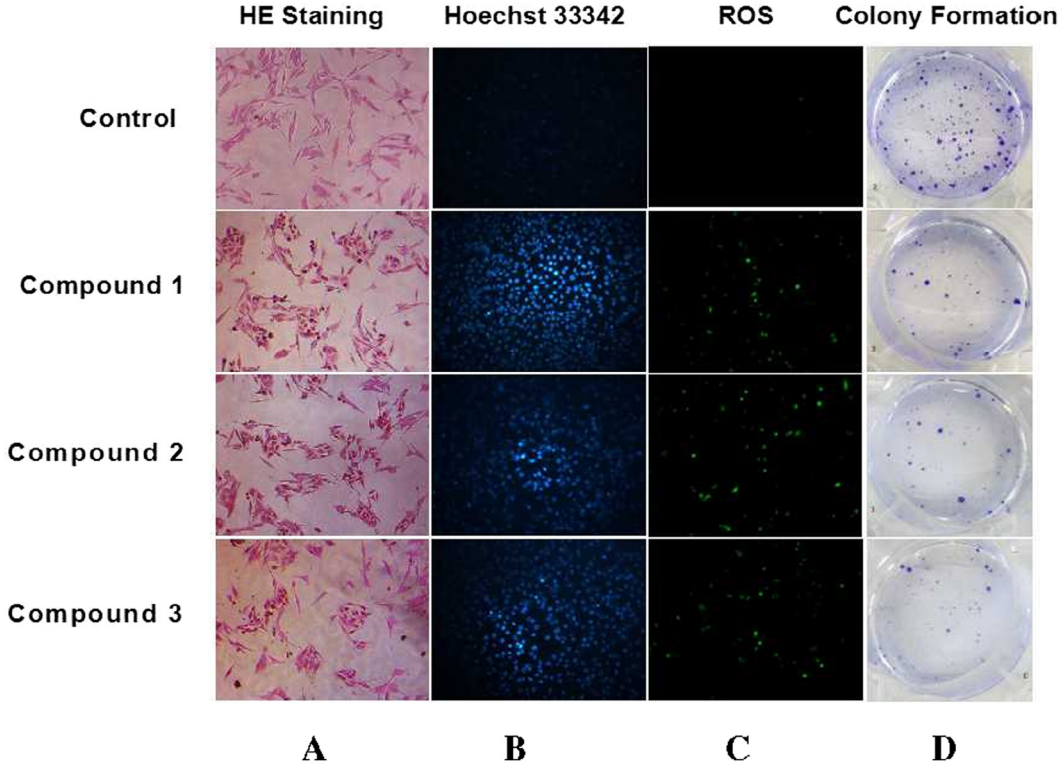

Fig. 9. A and B are morphological changes in the nuclei (apoptosis) of MDA-MB-231 cells treated with **1**–**3** for 24 h, respectively, followed with HE and Hoechst 33342 staining. **C** is ROS generation assay in MDA-MB-231 cancer cells after treatment with 1–3 for 24 h respectively. D is the multiplication inhibition of MDA-MB-231 cell treated with **1**–**3** for 24 h respectively.

applied. As shown in Fig. 9C, cells were exposed to **1**–**3** at concentration of 1 μM for 24 h, samples were observed under a fluorescent microscope (Olympus) at 100X magnification. Strong green fluorescence indicating the generation of ROS was observed compared with the control group, which suggested that ROS generated from these Cu(II) compounds could be the possible reason for cell apoptosis.

Annexin V-FITC/PI dual staining was carried out to detect complexes induced apoptosis in MDA-MB-231 cells. As shown in Fig. 10 (A-D), the complexes treatments resulted in apoptosis rates

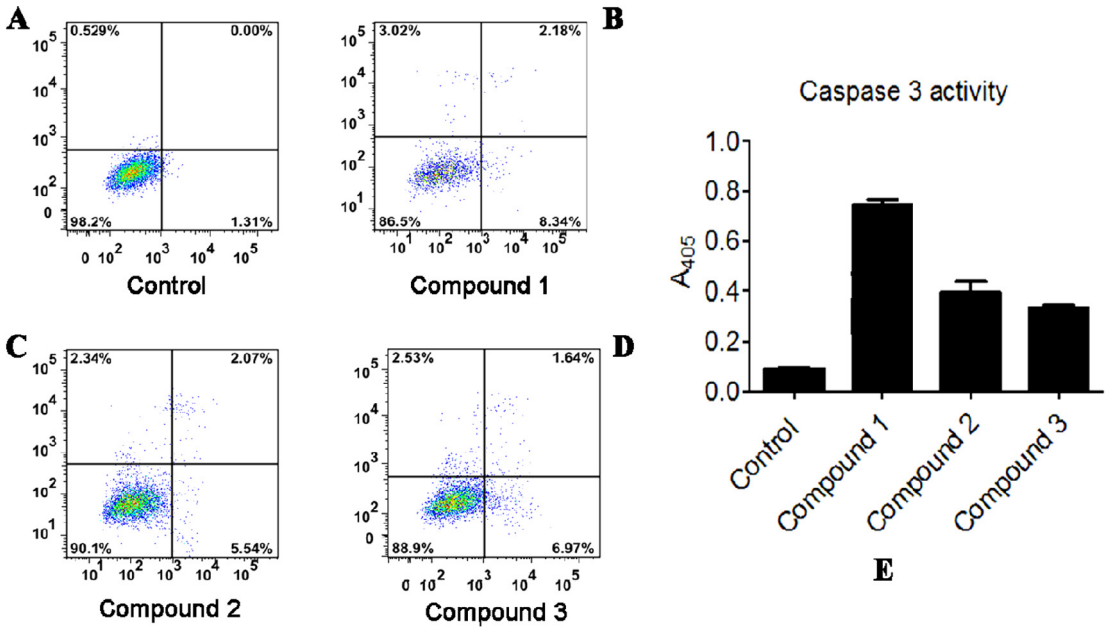

Fig. 10. Annexin V-FITC/PI staining (A–D) detected apoptosis in MDA-MB-231 cells after treatment with **1**–**3** for 24 h at the selected concentration by MTT assay. E showed the Caspase-3 activity about **1**–**3**.

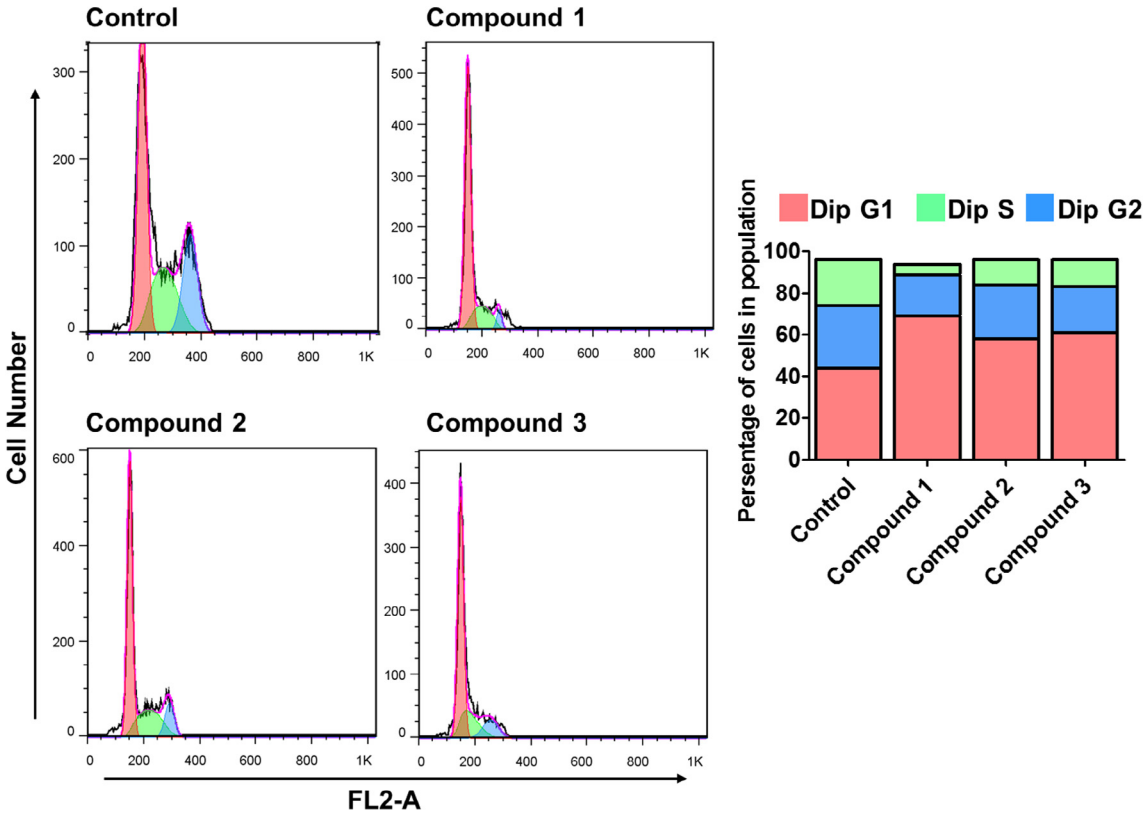

Fig. 11. (1) Cell cycle analysis using flow cytometry was carried on MDA-MB-231 cells treated with **1**–**3** for 24 h at the selected concentration by MTT assay. (2) The percentages of MDA-MB-231 cancer cells in the different phases of cell cycle were presented.

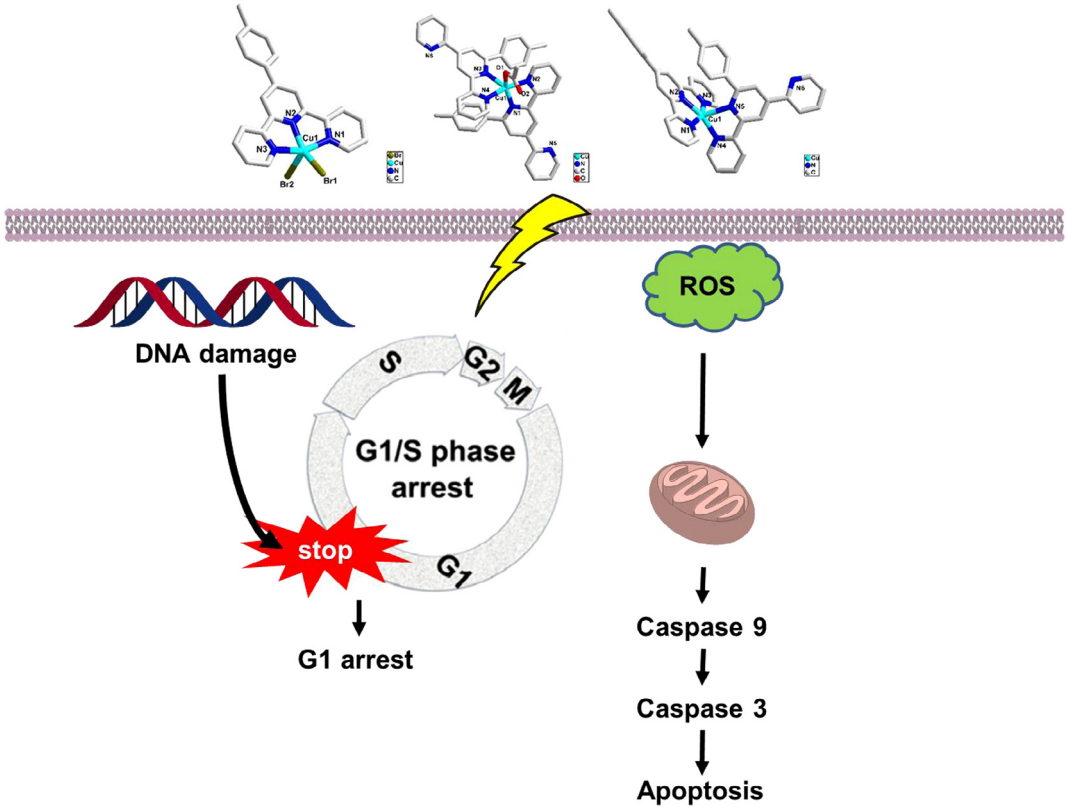

Fig. 12. Proposed anti-cancer mechanisms of **1**–**3**.

of 10.52 ± 0.23% for **1**, 7.61 ± 0.17% for **2**, 8.61 ± 0.34% for **3**, respectively, all of which were statistically different from the control. The complexes induced apoptosis was further analyzed by examining the mRNA expression of caspase family using quantitive PCR shown in Fig. S7. Increased caspase 9 and caspase 3 expression were positively correlated with the apoptotic rate when treated with **1**–**3** for 24 h, respectively, while caspase 8 was downregulated. And the Caspase-3 activity of MDA-MB-231 cells was further detected using Caspase-3 colorimetric assay. As shown in Fig. 10 (E), the three complexes upregulated the caspase-3 activities in MDA-MB-231 cells. Among these three complexes, **1** showed strongest ability of Caspase-3 activation compared with **2** and **3** at the same concentration. Thus, Caspase-3-induced apoptosis might be the possible mechanism of these complexes induced cell apoptosis and death.

Cell cycle distributions of MDA-MB-231 cells at different stages were determined using flow cytometry (FCM). Cells were treated with these three compounds at IC_{50} value for 24 h, individually. As shown in Fig. 11(1), although a lot of parallel experiments had been done, signals for sub-G1 peaks related to the presence of apoptosis were rarely observed, which was different from the previously reported literature [72]. However, as shown in Fig. 11(2), the population in S and G_2/M phases declined significantly, combined with a dramatic increase in G_0/G_1 phase, respectively, suggesting that these three copper complexes arrested the MDA-MB-231 cell at the G_0/G_1 phase of cell cycle.

According to data mentioned above, we speculated the proposed anti-cancer mechanisms of **1**–**3**, as shown in Fig. 12. When treated with these complexes, DNA damage would be induced which led to the G1 arrest in cancer cells. At the same time, the formation of ROS activated the caspase family mediated mitochondrial apoptotic pathway.

4. Conclusion

Three Cu(II) complexes with two isomer ligands obtain N atoms were synthesized and characterized. X-ray crystallography structure showed that three Cu(II) ions had the same five-coordinated mode and they were all mononuclear compounds with monoclinic $p\bar{1}$ space group. The space configuration of three complexes was square-pyramid because the value of τ was equal to 0.09 for **1**, 0.06 for **2** and 0.07 for **3**. Those three complexes were characterized in DMF solution by using ESI-MS: to **1**, 466.99 for $[Cu(\mathbf{L^1})(Br)]^+$; to **2**, 709.21 for $[Cu(\mathbf{L^2})_2\text{-}H]^+$ and to **3**, 709.21 for $[Cu(\mathbf{L^1})(\mathbf{L^2})\text{-}H]^+$. The result of ESI-MS showed that the small molecule ion (Br^- in **1** and $CH3COO^-$ in **2**) leaved from complex in DMF solution. The binding ability of complexes to DNA was measured by UV-visible spectroscopy, fluorescence spectral titration and viscosity measurements, which showed three complexes could bind to DNA in a slightly strong binding affinity with $K_b = 6.36 \times 10^5$ for **1**, $K_b = 3.82 \times 10^5$ for **2** and $K_b = 1.26 \times 10^4$ for **3**. A series of spectrum experiments of three Cu(II) complexes with BSA showed that complexes could combine with BSA very well. Gel electrophoresis experiment showed that **1**–**3** had excellent DNA cleavage activities in the absence of exogenous oxidants, and **2** exhibited the best DNA cleavage activity among all complexes. Moreover, three cooper complexes could generate singlet oxygen ($^1O_2$) as the ROS during the DNA cleavage process in the natural light under an aerobic environment, the more accurate DNA cleavage mechanism of the three complexes needs further exploration, such as: anaerobic experiment, light avoidance test and so on. MTT assay gave a result that **1**–**3** had the lower IC_{50} value than cisplatin, and HE, Hoechst 33342 and Annexin V-FITC/PI staining assays demonstrated their anti-cancer effects of promoting G1 arrest and inducing apoptosis. Further studies indicated that the inhibited proliferation ability on

cancer cells yielded by these complexes was achieved through the production of reactive oxygen species (ROS) and the activation of Caspase-3. Besides, further study of the chiral enantiomers in pharmacological activities was worth carrying out.

Acknowledgements

This work was supported by the National Natural Science Foundation of China (21171101, 21071083 and 21471085) and MOE Innovation Team (IRT 13022) of China.

Appendix A. Supplementary data

Electronic supplementary information (ESI) available. CCDC 1471418–1471420. Supplementary data associated with this article can be found, in the online version, at http://dx.doi.org/10.1016/j.ica.2016.12.002.

References

[1] M. Russo, G. Siravegna, L.S. Blaszkowsky, et al., Cancer Discov. 6 (2015) 147–154.
[2] S.H.C. Cheng, B.L. Yu, C.F. Horng, S.Y. Tsai, C.M. Chen, N.M. Chu, M.H. Tsou, C.K.J. Lin, L.S. Shih, M.C. Liu, J. Cancer Res. Prac. 3 (2016) 1–8.
[3] B. Rosenberg, L. VanCamp, J.E. Trosko, V.H. Mansour, Platinum compounds: a new class of potent antitumour agents, Nature 222 (1969) 385–386.
[4] E.R. Jamieson, S.J. Lippard, Chem. Rev. 99 (1999) 2467–2498.
[5] B. Rosenberg, L. VanCamp, Cancer Res. 30 (1970) 1799–1802.
[6] P. Heffeter, U. Jungwirth, M. Jakupec, C. Hartinger, M. Galanski, L. Elbling, M. Micksche, B. Keppler, W. Berger, Drug Resist. Update 11 (2008) 1–16.
[7] K.D. Mjos, C. Orvig, Chem. Rev. 114 (2014) 4540–4563.
[8] R. Drmanac, A.B. Sparks, M.J. Callow, A.L. Halpern, et al., Science 327 (2010) 78–81.
[9] S.I. Nakano, D. Miyoshi, N. Sugimoto, Chem. Rev. 114 (2014) 2733–2758.
[10] G.Q. Zheng, Y. Fu, C. He, Chem. Rev. 114 (2014) 4602–4620.
[11] S. Dhar, D. Senapati, P.K. Das, P. Chattopadhyay, M. Nethaji, A.R. Chakravarty, J. Am. Chem. Soc. 125 (2003) 12118–12123.
[12] S. Sharma, S.K. Singh, M. Chandra, D.S. Pandey, J. Inorg. Biochem. 99 (2005) 458–466.
[13] A. Hussain, K. Somyajit, B. Banik, S. Banerjee, G. Nagaraju, A.R. Chakravarty, Dalton Trans. 42 (2013) 182–195.
[14] B. Banik, P.K. Sasmal, S. Roy, R. Majumdar, R.R. Dighe, A.R. Chakravarty, Eur. J. Inorg. Chem. (2011) 1425–1435.
[15] S. Roy, S. Roy, S. Saha, R. Majumdar, R.R. Dighe, E.D. Jemmis, A.R. Chakravarty, Dalton Trans. 40 (2011) 1233–1242.
[16] Q. Jiang, J.H. Zhu, Y.M. Zhang, Z.J. Guo, Biometals 22 (2009) 297–305.
[17] S. Roy, S. Saha, R. Majumdar, R.R. Dighe, A.R. Chakravarty, Polyhedron 29 (2010) 3251–3256.
[18] J. He, P. Hu, Y.J. Wang, M.L. Tong, H.Z. Sun, Z.W. Mao, L.N. Ji, Dalton Trans. (2008) 3207–3214.
[19] E.I. Solomon, P. Chen, M. Metz, S.K. Lee, A.E. Palmer, Angew. Chem. Int. Ed. 40 (2001) 4570–4590.
[20] C. Santini, M. Pellei, V. Gandin, M. Porchia, F. Tisato, C. Marzano, Chem. Rev. 114 (2014) 815–862.
[21] M.N. Patel, H.N. Joshi, C.R. Patel, Polyhedron 40 (2012) 159–167.
[22] B.Z. Momeni, S. Heydari, Polyhedron 97 (2015) 94–102.
[23] J.A. Denny, M.Y. Darensbourg, Chem. Rev. 115 (2015) 5248–5273.
[24] C. Bhaumik, S. Das, D. Saha, S. Dutta, S. Baitalik, Inorg. Chem. 49 (2010) 5049–5062.
[25] L.X. Zhao, T.S. Kim, S.H. Ahn, T.H. Kim, E.K. Kim, W.J. Cho, H. Choi, C.S. Lee, J.A. Kim, T.C. Jeong, C.E.S. Lee, Bioorg. Med. Chem. Lett. 11 (2001) 2659–2662.
[26] V. Uma, M. Elango, B.U. Nair, Eur. J. Inorg. Chem. (2007) 3484–3490.
[27] M.N. Patel, D.S. Gandhi, P.A. Parmar, Spectrochim. Acta A. 84 (2011) 243–248.
[28] W. Zhou, X.Y. Wang, M. Hu, C.C. Zhu, Z.J. Guo, Chem. Sci. 5 (2014) 2761–2770.
[29] S. Rajalakshmi, T. Weyhermüller, A.J. Freddy, H.R. Vasanthi, B. Unni Nair, Eur. J. Med. Chem. 46 (2011) 609–617.
[30] V.M. Manikandamathavan, R.P. Parameswari, T. Weyhermüller, H.R. Vasanthi, B. Unni Nair, Eur. J. Med. Chem. 46 (2011) 4537–4547.
[31] W. Zhou, X.Y. Wang, M. Hu, C.C. Zhu, Z.J. Guo, J. Inorg. Biochem. 121 (2013) 114–120.
[32] A. Lewis, M. McDonald, S. Scharbach, S. Hamaway, M. Plooster, K. Peters, K.M. Fox, L. Cassimeris, J.M. Tanski, L.A. Tyler, J. Inorg. Biochem. 157 (2016) 52–61.
[33] M.A. Ragheb, M.A. Eldesouki, M.S. Mohamed, Spectrochim. Acta A Mol. Biomol. Spectrosc. 138 (2015) 585–595.
[34] C.N. Sudhamani, H.S. Bhojya Naik, K.R. Sangeetha Gowda, M. Giridhar, D. Girija, P.N. Prashanth Kumar, Spectrochim. Acta A: Mol. Biomol. Spectrosc. 138 (2015) 780–788.
[35] M. Salimi, K. Abdi, H.M. Kandelous, H. Hadadzadeh, K. Azadmanesh, A. Amanzadeh, H. Sanati, Biometals 28 (2015) 267–278.
[36] R. Dhivya, R. Dhivya, A. Riyasdeen, M. Palaniandavar, G. Mathan, M.A. Akbarsha, Biometals 28 (2015) 929–943.
[37] E. Rajalakshmanan, V. Alexander, Inorg. Chem. 46 (2007) 6252–6260.
[38] D.J. Bray, J.K. Clegg, K.A. Jolliffe, L.F. Lindoy, G. Wei, J. Coord. Chem. 61 (2008) 3–13.
[39] G.M. Sheldrick, C Software, University of Göttingen, Germany, 1996.
[40] G.M. Sheldrick, Acta Crystallogr., Sect. A 64 (2008) 112–122.
[41] J. Marmur, J. Mol. Biol. 3 (1961) 208–216.
[42] M.E. Reichmann, S.A. Rice, C.A. Thomas, P. Doty, J. Am. Chem. Soc. 76 (1954) 3047–3053.
[43] G. Cohen, H. Eisenberg, Biopolymers 8 (1969) 45–55.
[44] C.N. Sudhamani, H.S. Bhojya Naik, D. Girija, K.R. Sangeetha Gowda, M. Giridhar, T. Arvinda, Spectrochim. Acta A 118 (2014) 271–278.
[45] F. Gao, H. Chao, F. Zhou, Y.X. Yuan, B. Peng, L.N. Ji, J. Inorg. Biochem. 100 (2006) 1487–1494.
[46] A.W. Addison, T.N. Rao, J. Reedijk, J.V. Rijn, G.C. Verschoor, J. Chem. Soc. Dalton Trans. (1984) 1349–1356.
[47] J. Lu, Q. Sun, J.L. Li, L. Jiang, W. Gu, X. Liu, J.L. Tian, S.P. Yan, J. Inorg. Biochem. 137 (2014) 46–56.
[48] V.M. Manikandamathavan, V. Rajapandian, A.J. Freddy, T. Weyhermüller, V. Subramanian, B.U. Nair, Eur. J. Med. Chem. 57 (2012) 449–458.
[49] Y. Gou, Z. Zhang, J.X. Qi, S.C. Liang, Z.P. Zhou, F. Yang, H. Liang, J. Inorg. Biochem. 153 (2015) 13–22.
[50] C.N. Sudhamani, H.S.B. Naik, K.R.S. Gowda, M. Giridhar, D. Girija, P.N.P. Kumar, Spectrochim. Acta. A. 138 (2015) 780–788.
[51] X.Q. Zhou, Q. Sun, L. Jiang, S.T. Li, W. Gu, J.L. Tian, X. Liu, S.P. Yan, Dalton Trans. 14 (2015) 9516–9522.
[52] V. Uma, M. Kanthimathi, T. Weyhermuller, B.U. Nair, J. Inorg. Biochem. 99 (2005) 2299–2304.
[53] M.T. Carter, M. Rodriguez, A.J. Bard, J. Am. Chem. Soc. 111 (1989) 8901–8905.
[54] V.M. Manikandamathavan, T. Weyherm üller, R.P. Parameswari, M. Sathishkumar, V. Subramanian, Balachandran Unni Nair, Dalton Trans. 43 (2014) 13018–13031.
[55] V.M. Manikandamathavan, B. Unni Nair, Eur. J. Med. Chem. 68 (2013) 244–252.
[56] J.R. Lakowicz, G. Weber, Biochemistry 12 (1973) 4161–4170.
[57] B.C. Baguley, M. Le Bret, Biochemistry 23 (1984) 937–943.
[58] S. Dhar, M. Nethaji, A.R. Chakravarty, J. Inorg. Biochem. 99 (2005) 805–812.
[59] P. Ramadevi, R. Singh, S.S. Jana, R. Devkar, D. Chakraborty, J. Photoch. Photobio. A. 305 (2015) 1–10.
[60] R.F. Pasternack, M. Caccam, B. Keogh, T.A. Stephenson, A.P. Williams, E.J. Gibbs, J. Am. Chem. Soc. 113 (1991) 6835–6840.
[61] A. Kumar, J.P. Chinta, A.K. Ajay, M.K. Bhat, C.P. Rao, Dalton Trans. 40 (2011) 10865–10872.
[62] N. Shahabadi, S. Kashanian, F. Darabi, Eur. J. Med. Chem. 45 (2010) 4239–4245.
[63] D.J. Li, M. Zhu, C. Xu, B.M. Li, Eur. J. Med. Chem. 46 (2011) 588–599.
[64] A. Patra, T.K. Sen, A. Ghorai, G.T. Musie, S.K. Mandal, U. Ghosh, M. Bera, Inorg. Chem. 52 (2013) 2880–2890.
[65] B.K. Paul, A. Samanta, N. Guchhait, J. Phys. Chem. B. 114 (2010) 6183–6195.
[66] Y.Q. Wang, H.M. Zhang, G.C. Zhang, W.H. Tao, S.H. Tang, J. Lumn. 126 (2007) 211–218.
[67] S. Ghosh, S. Jana, N. Guchhait, J. Phys. Chem. B. 116 (2012) 1155–1163.
[68] J. Shao, Z.Y. Ma, A. Li, Y.H. Liu, C.Z. Xie, Z.Y. Qiang, J.Y. Xu, J. Inorg. Biochem. 136 (2014) 13–23.
[69] G. Chandrasekher, D. Sailaja, Invest. Ophthalmol. Vis. Sci. 45 (2004) 3565–3577.
[70] K. Sinha, J. Das, P.B. Pal, P.C. Sil, Arch. Toxicol 87 (2013) 1157–1180.
[71] P. Li, Q.L. Zhao, L.H. Wu, P. Jawaid, Y.F. Jiao, M. Kadowaki, T. Kondo, Apoptosis 19 (2014) 1043.
[72] M. Kracikova, G. Akiri, A. George, R. Sachidanandam, S.A. Aaronson, Cell Death Differ. 20 (2013) 576–588.